# A computationally-guided non-equilibrium synthesis approach to materials discovery in the SrO-Al2O3-SiO2 phase field

Euan M. Duncan, Amandine Ridouard, Franck Fayon, Emmanuel Veron, Cécile Genevois, Mathieu Allix, Christopher Collins, Michael J Pitcher

# A computationally-guided non-equilibrium synthesis approach to materials discovery in the $SrO$-$Al_2O_3$-$SiO_2$ phase field

Euan M. Duncan,[a] Amandine Ridouard,[a] Franck Fayon,[a] Emmanuel Veron,[a] Cécile Genevois,[a] Mathieu Allix,[a] Christopher M. Collins,*[b] and Michael J. Pitcher*[a]

[a] *CEMHTI, CNRS UPR3079, 1d Ave. de la Recherche Scientifique, 45071 Orléans, France.*
[b] *Department of Chemistry, Materials Innovation Factory, University of Liverpool, Liverpool L7 3NY, U.K.*

*Correspondence: c.m.collins@liverpool.ac.uk, michael.pitcher@cnrs-orleans.fr

**Abstract**

Glass-crystallisation synthesis is coupled to probe structure prediction for the guided discovery of new metastable oxides in the $SrO$-$Al_2O_3$-$SiO_2$ phase field, yielding a new ternary ribbon-silicate, $Sr_2Si_3O_8$. In principle, this methodology can be applied to a wide range of oxide chemistries by selecting an appropriate non-equilibrium synthesis route.

The discovery of inorganic oxides with new compositions and crystal structures is a key challenge in materials chemistry, with many domains in which new functional materials are required to enable advances in performance, cost or sustainability. When searching for new complex (ternary or higher) oxides, two important limiting factors are the intrinsic tendency of high-temperature ceramic synthesis to promote formation of the most thermodynamically stable phases, and the vast number of potential compositions for exploration. Together, these factors complicate attempts to identify and isolate new metastable materials, and render exhaustive searches impractical even for fairly limited phase fields.[1] Solutions to these problems have focused on alternative synthesis approaches that operate under conditions that are more amenable to the formation of non-equilibrium phases (e.g. chimie douce,[2] molten salt,[3] co-metathesis[4] or diverse solution-based processes[5]), on rapid automated characterisation,[6] and increasingly on materials-by-design approaches based on crystal structure prediction[7] and machine learning[8] that allow synthetic efforts to be concentrated on a manageable number of targets. Predictive and non-equilibrium synthesis methods are commonly applied in isolation, but the possibility of combining their respective advantages can enable new types of problems to be approached, such as the guided synthesis of new metastable oxide polymorphs,[9] which have so far received less attention.

Here, we tackle the metastability and combinatorial problems together by combining the probe structure (PS) compositional prediction approach[10,11] with glass-crystallisation (GC) as a non-equilibrium synthesis technique, for the guided discovery of new metastable compounds in the previously well-explored SrO-$Al_2O_3$-$SiO_2$ phase field. The PS approach aids the synthetic exploration of complex phase diagrams by mapping the most energetically-favourable regions for crystalline phase formation, and has previously been harnessed to conventional ceramic synthesis methods.[10] It is also suited to the discovery of metastable materials, which exist in local energy minima that are close to the convex hull,[12] as demonstrated recently by the isolation of the aperiodic titanate $Ba_{10}Y_6Ti_4O_{27}$ by careful optimisation of a ceramic synthesis protocol.[13] However, PS calculations have not previously been harnessed to a non-equilibrium synthesis route to target metastable compounds intentionally. Such an approach is expected to raise the energy threshold above the convex hull at which synthesisable compounds might be attainable, increasing the probability of new compounds being accessible in a given phase field.

GC is a non-equilibrium synthesis method that can yield metastable oxides with extraordinary compositions[14] or entirely new structure types.[15] Its capability is enhanced by the use of containerless synthesis methods[16] that allow a wide range of compositions to be vitrified, including highly atypical glass-formers,[17–19] which can then be crystallised at moderate temperatures. GC is complementary to other non-equilibrium methods, which can provide alternative routes to the same metastable phases.[20,21] By selecting a phase field with a broad glass-forming region, GC can be coupled effectively to the PS approach in a systematic search for new compounds. In this context, the SrO-$Al_2O_3$-$SiO_2$ phase field is an ideal test case: most of the phase space can be vitrified,[22] and it is known to host functional materials such as luminescence phosphor hosts[23–25] and transparent ceramics.[26,27] Furthermore, the possibility of isolating new metastable compounds in this system has been demonstrated by the GC synthesis of $SrAl_2SiO_6$, which exists in the solid solution gap between two transparent ceramic tectosilicate families on the $SrAl_2O_4$ – $SiO_2$ tie-line, and adopts a unique structure type.[28]

Encouraged by the realisation of such new and complex oxides in the SrO-$Al_2O_3$-$SiO_2$ phase field by GC, we conducted a probe-structure analysis using FUSE[11] to identify other fertile regions for exploration. Probe structure calculations were performed on the whole SrO-$Al_2O_3$-$SiO_2$ phase field, for a total of 42

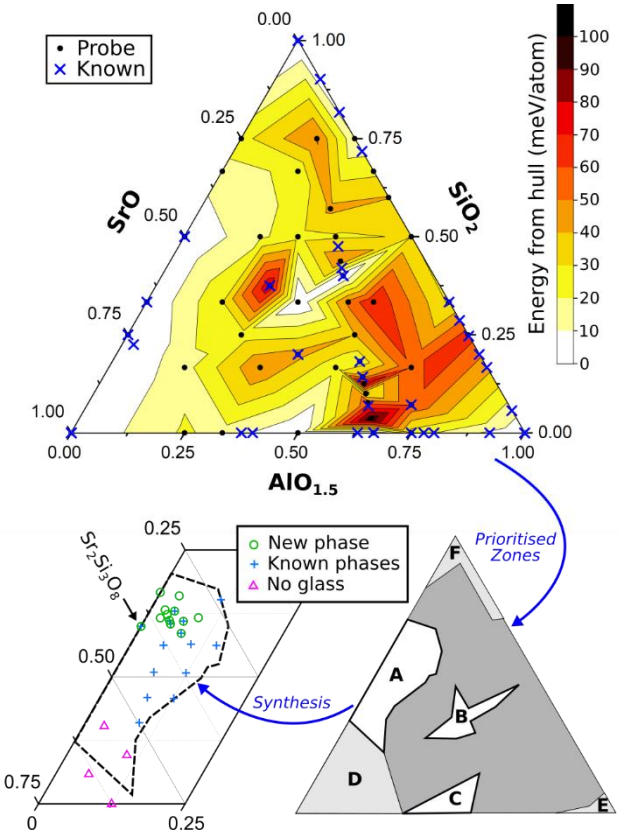


***Fig. 1*** *Convex hull calculated for the phase field SrO-$AlO_{1.5}$-$SiO_2$. The 42 probe structure compositions are plotted as black points, and blue crosses indicate known compounds from the equilibrium phase diagram and/or ICSD. Where two points coincide, the lower energy structure (probe or ICSD) was taken for the convex hull calculation. A full list of probe structures is available in Table S1. The lowest energy regions A-C were prioritised for exploration by glass-crystallisation synthesis, whilst other low energy regions D-F were not explored synthetically. Region A yielded a new phase which could not be indexed to a known compound (green circles).*

compositions. The calculations included 15 compositions on the $SrAl_2O_4$ – $SiO_2$ line, which is known to host a range of metastable cation-disordered crystalline phases:[25,26,28] their inclusion in the convex hull construction allows a threshold energy to be estimated for the formation of new metastable phases in this system. The resulting $SrAl_2O_4$ – $SiO_2$ energy profile is plotted in Figure S1 alongside its constituent probe structures, which all contain chemically-plausible corner-sharing tetrahedral aluminosilicate frameworks (consistent with the known structural chemistry of such materials) and reasonable coordination numbers for $Sr^{2+}$ (see Figure S2). The ability of FUSE to generate plausible structures at these compositions is highlighted at 40% $SiO_2$ ($SrAl_2Si_2O_8$), where the probe structure corresponds to a cation-ordered variant of the experimentally-obtained hexacelsian structure.[26] From the energy profile it can be seen that almost all of the known compounds on the $SrAl_2O_4$ – $SiO_2$ line lie within 50 meV/atom of the convex hull. The region 25 – 30% $SiO_2$, which hosts metastable $SrAl_2SiO_6$, lies approximately 40 meV/atom above the convex hull.

The calculated convex hull for the whole phase diagram is plotted in Figure 1. The energy surface exhibits several low-energy regions which cover a substantial fraction of the phase diagram: the application of a 35 meV/atom threshold for exploration (an arbitrary value used previously for stable oxides[10,11]) would entail an excessively broad experimental search (see Figure S3). In order to focus only on the most promising regions for experimental exploration, six candidate regions **A** – **F** were identified, corresponding only to the lowest calculated energies (< 20 meV/atom) as shown in Figure

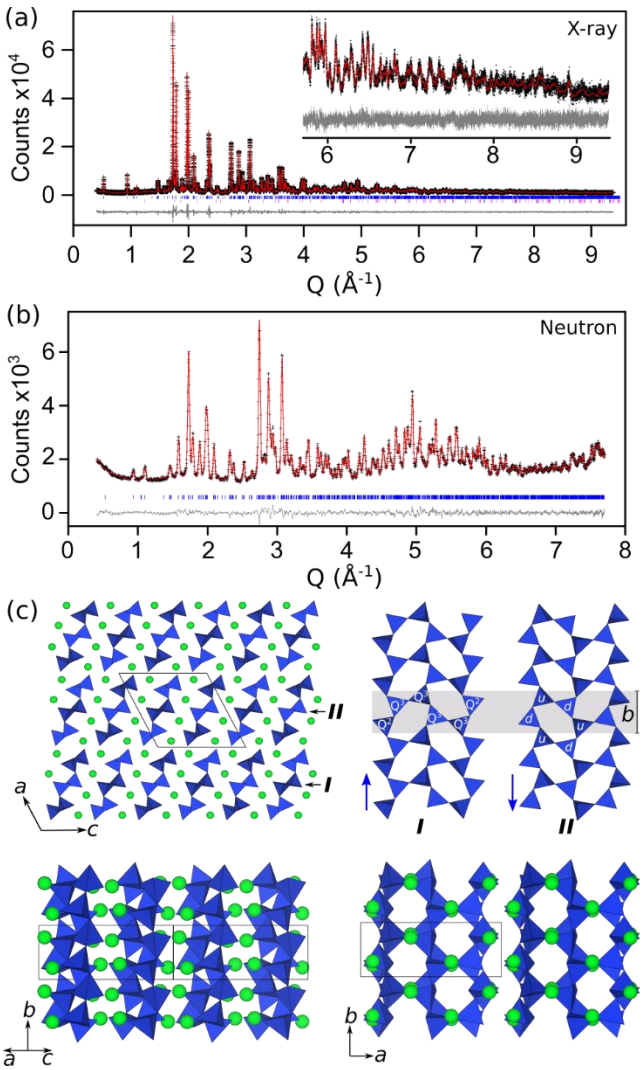


***Fig. 2*** *Crystal structure of $Sr_2Si_3O_8$, obtained by crystallisation of $Sr_{0.344}Al_{0.033}Si_{0.623}O_{1.64}$ glass at 900°C. Rietveld refinement against (a) SXRD data (λ = 0.45808 Å, $R_{wp}$ = 7.34 %, $\chi^2$ = 1.35) and (b) neutron diffraction data (λ = 1.5936 Å, $R_{wp}$ = 3.00 %, $\chi^2$ = 1.72). (c) Projections of the SXRD-refined structure showing an antiparallel arrangement of $[Si_6O_{16}]^{8-}$ ribbons, where **I** and **II** represent "up" and "down" orientations. Atoms = $Sr^{2+}$, tetrahedra = $[SiO_4]$.*

1. Regions **A – C** encompass compositions which are far from the vertices of the phase diagram, far from other known pseudo-ternaries, and amenable to glass formation, and these were selected for systematic synthesis trials. Conversely, the regions **D, E** and **F** were not explored experimentally due to the difficulty in vitrifying compositions close to SrO (**D**) and $Al_2O_3$ (**E**), and difficulty in crystallising $SiO_2$-rich compositions (**F**) at moderate temperatures.

To enable a consistent synthetic approach to the experimental phase search, standard synthesis conditions were defined for each region **A – C** by preparing 1 or 2 reference glasses from the centre of each region. These were then crushed into powder and their crystallisation temperatures ($T_C$) obtained by in-situ PXRD (the reference compositions and their crystallisation temperatures are shown in Figure S4). A spread of trial glass compositions was then synthesised according to these conditions, with crystallisations performed ex-situ for 1 hour (see Methods). In regions **B** and **C**, glass synthesis was successful for all trial compositions, but the crystallisation steps produced only mixtures of known compounds: **B** compositions crystallised predominantly into mixtures of $Sr_2Al_2SiO_7$ and feldspar-type $SrAl_2Si_2O_8$, whilst **C** compositions were dominated by a stuffed-tridymite phase resembling the nearby

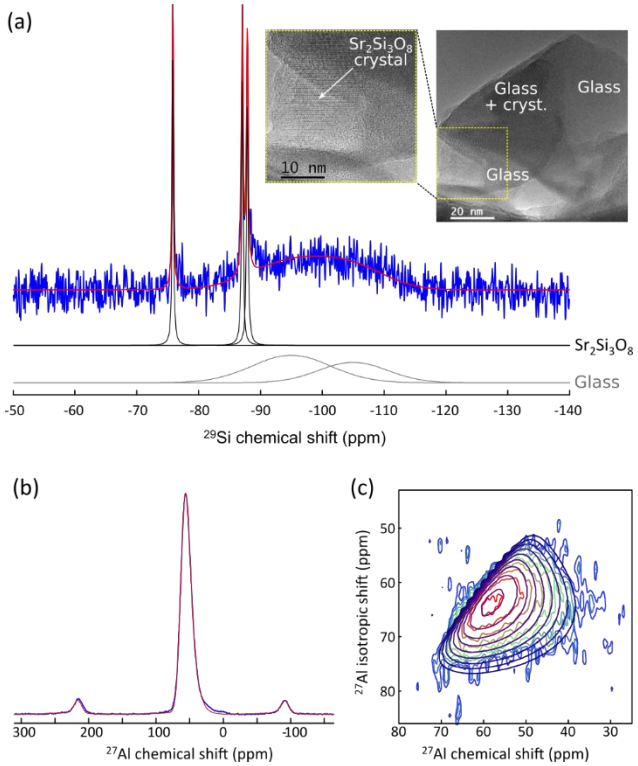


***Fig. 3*** *MAS-NMR spectra of $Sr_2Si_3O_8$, crystallised from $Sr_{0.344}Al_{0.033}Si_{0.623}O_{1.64}$ glass. (a) $^{29}$Si spectrum showing sharp resonances from three inequivalent Si atoms in the $Sr_2Si_3O_8$ structure, with a $Q^2/Q^3$ ratio that agrees closely with the Rietveld model, and a broad resonance from amorphous Si in $Q^3$ and $Q^4$ configuration accounting for 58 % of the Si nuclei. Inset is a TEM image of a $Sr_2Si_3O_8$ crystal embedded in a glassy matrix, consistent with the NMR data. (b,c) 1D and 2D-MQMAS $^{27}$Al NMR showing only a single broad resonance typical of an amorphous phase.*

$Sr_{0.9}Al_{1.8}Si_{0.2}O_4$[25] (see Figure S5). In contrast, initial exploration of region **A** yielded several samples whose multi-component PXRD patterns, generally dominated by $SrSiO_3$, contained a new pattern that could not be indexed to a known phase. By refining the target composition systematically, this new PXRD pattern was eventually isolated as the only crystalline phase at six different nominal compositions, as shown in Figure 1.

One of these compositions, $Sr_{0.344}Al_{0.033}Si_{0.623}O_{1.64}$, was crystallised at 900°C (see DSC, Figure S6) and selected for *ab initio* crystal structure solution due to its sharp Bragg peaks and the absence of secondary crystalline phases. High resolution SXRD data were collected at ambient temperature and indexed to a primitive monoclinic unit cell of dimensions $a$ = 13.327 Å, $b$ = 4.582 Å, $c$ = 13.464 Å and $\beta$ = 116.7° in space group $P2_1/c$. Using the same data set, the structure was then solved *ab initio* by simulated annealing of $Sr^{2+}$ ions and $[SiO_4]^{4-}$ rigid tetrahedra (see Supplementary Information). The resulting model provided excellent Rietveld fits to both SXRD (Figure 2a, Table S2) and neutron diffraction data (Figure 2b, Table S3). It is a one-dimensional structure whose main feature is a $[Si_6O_{16}]^{8-}$ ribbon, formed by three zweier chains that are linked into 6-membered rings of tetrahedra in *ududud* orientation. This generates two $Q^2$ (2-connected) and four $Q^3$ (3-connected) tetrahedra, as indicated in Figure 2c. The ribbon is polar along its propagation direction, but an antiparallel checkerboard-type packing arrangement produces a non-polar structure overall, as indicated by the blue arrows on ribbons ***I*** and ***II*** in Figure 2. Adjacent ribbons are separated by columns of $Sr^{2+}$ in 7-fold coordination. The structure is closely related to that of $Ba_2Si_3O_8$,[29] which features similar $[Si_6O_{16}]^{8-}$ ribbons. The two structure types differ in terms of their antiparallel ribbon packing modes, and by a significant ribbon

distortion in $Sr_2Si_3O_8$ corresponding to a large cooperative twist of the two external zweier chains (see Supplementary Information, section E).

The structural model has a different composition from the parent glass ($Sr_{0.344}Al_{0.033}Si_{0.623}O_{1.64}$), and offers no obvious mechanism for incorporating $Al^{3+}$. $^{29}Si$ and $^{27}Al$ MAS-NMR were used to confirm the crystal structure, and to investigate the fate of the $Al^{3+}$. Here, distinct narrow peaks at $^{29}Si$ isotropic chemical shifts of -75.9, -87.1 and -87.9 ppm with relative intensities in a 1:1:1 ratio indicate the presence of one $Q^2$ and two inequivalent $Q^3$ Si sites with the same multiplicities (Figure 3 and Figure S7), as expected from the structural model. Furthermore, the observed isotropic and anisotropic chemical shifts were very close to GIPAW-calculated values from the refined structure (Table S4), confirming the accuracy of the refined atomic positions. The $^{29}Si$ spectrum also features a broad resonance corresponding to an amorphous phase, whose chemical shift range is typical of $Q^3$ and $Q^4$ species found in silicate glasses, accounting for 58 % of the Si nuclei. At the same time, 1D and MQMAS $^{27}Al$ MAS-NMR spectra show line shapes typical of disordered $Al^{3+}$ in tetrahedral coordination, with no quadrupolar splitting, indicating that $Al^{3+}$ is present only in the amorphous phase. These conclusions are supported by TEM imaging and EDS (Figure 3(a) inset, and Table S5) showing $Sr_2Si_3O_8$ crystals embedded in a $SiO_2$-enriched glassy matrix.

In addition to heterogeneous crystallisation of alumina-containing precursor glasses, $Sr_2Si_3O_8$ can also be obtained directly by crystallisation of 0.40 SrO – 0.60 $SiO_2$ glass in the range 825 - 1050°C. Above 1050 °C, it decomposes rapidly to the equilibrium phases $SrSiO_3$ and $SiO_2$, illustrating its metastability (see *in situ* PXRD, Figure S8). This homogeneous crystallisation route yields samples of relatively low crystallinity with a substantial residual glass fraction, as shown by PXRD and $^{29}Si$ NMR (Figures S9 and S10). Attempts to improve the crystallinity by optimising temperature and annealing time had no significant effect on the PXRD peak widths, and tended to promote thermal decomposition (Figures S11 and S12). This difficulty in isolating fully-crystallised ceramic samples of $Sr_2Si_3O_8$ directly is surprising, given its apparent ease of crystallisation from alumina-containing precursor glasses, and may require an improved understanding of the crystallisation process before it can be overcome.

Probe structure prediction has been combined with a non-equilibrium synthesis method for the first time. In principle, this allows access to a greater range of new compounds than would be possible by exploring with a conventional ceramic synthesis method. The approach is validated by the discovery of $Sr_2Si_3O_8$, the first ambient-pressure example of a ternary strontium silicate with a polymerised [$SiO_4$] framework. $Sr_2Si_3O_8$ forms readily by heterogeneous crystallisation of alumina-containing glass precursors, yielding glass-ceramics of sufficient crystalline quality for *ab initio* structure solution. It can also be prepared with lower crystalline quality by homogeneous crystallisation of 0.40 SrO – 0.60 $SiO_2$ glass. $Sr_2Si_3O_8$ may be of interest for scintillation or luminescence properties,[30,31] but an improved synthesis protocol is required to obtain fully-crystallised samples suitable for functionalisation. The experimental focus on very low calculated energy regions (< 20meV/atom) in this study is non-exhaustive and may leave scope for the discovery of other metastable compounds at higher energy thresholds (e.g. < 50meV/atom). The PS-GC methodology can be applied directly to other glass-forming phase fields, and can be extended to non-glass-forming systems by using alternative non-equilibrium synthesis routes.

**Conflicts of interest**

There are no conflicts to declare.

**Acknowledgements**

Funding was provided by the ANR (grant 20-CE08-0007), EPSRC (grant EP/N004884), and PHC-ALLIANCE (grant 44791ZG). DSC data were collected by Sandra Ory (CEMHTI). Neutron data were collected by Dr. Stanislav Savvin (ILL, Grenoble, France). Use of the Advanced Photon Source at Argonne National Laboratory was supported by the U. S. Department of Energy, Office of Science, Office of Basic Energy Sciences, under Contract No. DE-AC02-06CH11357. Computing resources were provided by the University of Liverpool.

**Notes and references**

1 D. W. Davies, K. T. Butler, A. J. Jackson, A. Morris, J. M. Frost, J. M. Skelton and A. Walsh, *Chem*, 2016, **1**, 617–627.
2 J. Gopalakrishnan, *Chem. Mater.*, 1995, **7**, 1265–1275.
3 D. Portehault, S. Delacroix, G. Gouget, R. Grosjean and T. H. C. Chan-Chang, *Acc. Chem. Res.*, 2018, **51**, 930–939.
4 P. K. Todd and J. R. Neilson, *J. Am. Chem. Soc.*, 2019, **141**, 1191–1195.
5 D. L. M. Cordova and D. C. Johnson, *ChemPhysChem*, 2020, **21**, 1345–1368.
6 J. Li, C. Lin, Y. Min, Y. Yuan, G. Li, S. Yang, P. Manuel, J. Lin and J. Sun, *J. Am. Chem. Soc.*, 2019, **141**, 4990–4996.
7 A. R. Oganov, C. J. Pickard, Q. Zhu and R. J. Needs, *Nat. Rev. Mater.*, 2019, **4**, 331–348.
8 J. Schmidt, M. R. G. Marques, S. Botti and M. A. L. Marques, *npj Comput. Mater.*, 2019, **5**, 1–36.
9 A. Parija, G. R. Waetzig, J. L. Andrews and S. Banerjee, *J. Phys. Chem. C*, 2018, **122**, 25709–25728.
10 C. Collins, M. S. Dyer, M. J. Pitcher, G. F. S. Whitehead, M. Zanella, P. Mandal, J. B. Claridge, G. R. Darling and M. J. Rosseinsky, *Nature*, 2017, **546**, 280–284.
11 C. Collins, G. R. Darling and M. J. Rosseinsky, *Faraday Discuss.*, 2018, **211**, 117–131.
12 M. Aykol, S. S. Dwaraknath, W. Sun and K. A. Persson, *Sci. Adv.*, 2018, **4**, eaaq0148.
13 C. M. Collins, L. M. Daniels, Q. Gibson, M. W. Gaultois, M. Moran, R. Feetham, M. J. Pitcher, M. S. Dyer, C. Delacotte, M. Zanella, C. A. Murray, G. Glodan, O. Pérez, D. Pelloquin, T. D. Manning, J. Alaria, G. R. Darling, J. B. Claridge and M. J. Rosseinsky, *Angew. Chem., Int. Ed.*, 2021, **60**, 16457–16465.
14 W. Cao, A. I. Becerro, V. Castaing, X. Fang, P. Florian, F. Fayon, D. Zanghi, E. Veron, A. Zandonà, C. Genevois, M. J. Pitcher and M. Allix, *Adv. Funct. Mater.*, 2023, **33**, 2213418.
15 M. Allix, S. Alahrache, F. Fayon, M. Suchomel, F. Porcher, T. Cardinal and G. Matzen, *Adv. Mater.*, 2012, **24**, 5570–5575.
16 C. J. Benmore and J. K. R. Weber, *Advances in Physics: X*, 2017, **2**, 717–736.
17 K. Yoshimoto, A. Masuno, H. Inoue and Y. Watanabe, *J. Am. Ceram. Soc.*, 2012, **95**, 3501–3504.
18 J. Yu, Y. Arai, T. Masaki, T. Ishikawa, S. Yoda, S. Kohara, H. Taniguchi, M. Itoh and Y. Kuroiwa, *Chem. Mater.*, 2006, **18**, 2169–2173.
19 A. Masuno, S. Kohara, A. C. Hannon, E. Bychkov and H. Inoue, *Chem. Mater.*, 2013, **25**, 3056–3061.
20 J. Fan, V. Sarou-Kanian, X. Yang, M. Diaz-Lopez, F. Fayon, X. Kuang, M. J. Pitcher and M. Allix, *Chemistry of Materials*, 2020, **32**, 9016–9025.
21 Y. Zhang, L. Zhao, Z. Ye and Y. Zeng, *J. Adv. Ceram.*, 2022, **11**, 1613–1625.
22 D. Bahat, *J. Mater. Sci.*, 1969, **4**, 855–860.
23 S. Kubota, H. Yamane and M. Shimada, *Chem. Mater.*, 2002, **14**, 4015–4016.
24 S. Ye, Z.-S. Liu, X.-T. Wang, J.-G. Wang, L.-X. Wang and X.-P. Jing, *J. Lumin.*, 2009, **129**, 50–54.
25 A. J. Fernandez-Carrion, K. Al Saghir, E. Veron, A. I. Becerro, F. Porcher, W. Wisniewski, G. Matzen, F. Fayon and M. Allix, *Inorg. Chem.*, 2017, **56**, 14446–14458.
26 K. Al Saghir, S. Chenu, E. Veron, F. Fayon, M. Suchomel, C. Genevois, F. Porcher, G. Matzen, D. Massiot and M. Allix, *Chem. Mater.*, 2015, **27**, 508–514.

27 V. Castaing, C. Monteiro, A. D. Sontakke, K. Asami, J. Xu, A. J. Fernández-Carrión, M. G. Brik, S. Tanabe, M. Allix and B. Viana, *Dalton Trans.*, 2020, **49**, 16849–16859.
28 W. Wisniewski, A. J. Fernández-Carrión, P. Schöppe, C. Rüssel and M. Allix, *CrystEngComm*, 2018, **20**, 3455–3466.
29 K. F. Hesse and F. Liebau, *Z. Kristallogr. - New Cryst. Struct.*, 1980, **153**, 3–17.
30 Y. Eagleman, E. Bourret-Courchesne and S. E. Derenzo, *IEEE Trans. Nucl. Sci.*, 2012, **59**, 479–486.
31 M. Chen, Z. Xia, M. S. Molokeev and Q. Liu, *J. Mater. Chem. C*, 2015, **3**, 12477–12483.